Korean J. Chem. Eng., 34(9), 2406-2417 (2017)
DOI: 10.1007/s11814-017-0155-5

pISSN: 0256-1115
eISSN: 1975-7220

Novel polymorphous aluminosilicate nano minerals: Preparation, characterization and dyes wastewater treatment

Saleh Nosrati, Kumars Seifpanahi-Shabani†, and Mohammad Karamoozian

Faculty of Mining, Petroleum and Geophysics Engineering, Shahrood University of Technology, Shahrood, Iran
(*Received 7 November 2016 • accepted 31 May 2017*)

Abstract−Polymorphous aluminosilicate, such as Andalusite, Kyanite and Sillimanite, were prepared and characterized by XRF, XRD, FT-IR and SEM analysis. These cheap and accessible nanoparticles were used for removal of Disperse Red 177 and Disperse Blue 60 dyes. The adsorption process was held in a batch system considering the effects of major parameters consist of pH, adsorbent dosage, dye initial concentration and temperature. The obtained results show that both Freundlich and Temkin isotherms suitably fit with experimental data of adsorption of dyes in equilibrium mode. Also, the adsorption of dyes follows and matches pseudo-second-order kinetic model for Andalusite, Kyanite and Sillimanite nanoadsorbents. Thermodynamic study of dye adsorption process proves low randomness, exothermicity and spontaneous reactions. The comparison of three adsorbent efficiencies for adsorption of DR-177 and D-B-60 dyes was as: Andalusite>Sillimanite>Kyanite and Sillimanite>Kyanite>Andalusite, respectively.

Keywords: Andalusite, Kyanite and Sillimanite Nanominerals, Disperse Dyes Removal, Adsorption

INTRODUCTION

Dyes are of a great concern due to their being harmful to the environment, not only for humans but also for aquatic life. They are carcinogenic, mutagenic and allergenic. They also prevent sunlight penetration through water by absorption and reflection causing growth of bacteria and biological attacks [1-5]. Their discharge into the hydrosphere causes an unpleasant color and foul odor [5,6]. Many industries use dyes, such as paper, leather tanning, food processing, cosmetics, printing and so on [5-7]. Among them, textile industries are the most consumers of dyes [8,9]. Each year around 100 tons of dyes are discharged into water effluents [5].

Disperse dyes are used to color polyester, nylon, acetate, cellulose and acrylic. They are organic non-ionic compounds, nearly insoluble in water, applied in water by using a simple immersion technique which consumes large amount of water [10,11]. As a result, more than 40% of amount of dyes is not fixed to textile fibers [11]. Different methods have been used for removal of dyes including coagulation-flocculation [12], electrochemical treatment [13], membrane separation [14], biological treatment [15] and adsorption process [16-18]. Among them, adsorption is the most convenient method due to its low cost, simple operation and high efficiency [19-21]. The most commonly used adsorbent for industrial applications is activated carbon due to its high porosity and large surface area, which makes it effective [22]. But the cost of producing or regenerating activated carbon make it an expensive adsorbent [23,24]. This high cost has motivated the search for alternative economical and efficient adsorbents [6]. In addition, it has been announced that the use of activated carbon for disperse and vat dyes is inefficient [25,26].

Natural materials are among the adsorbents which have gained great attention due to their natural base and environmental friendly characteristics [27]. Quite a few of them have been reported being used as an adsorbent, such as perlite [28], diatomite [29], clay [30],

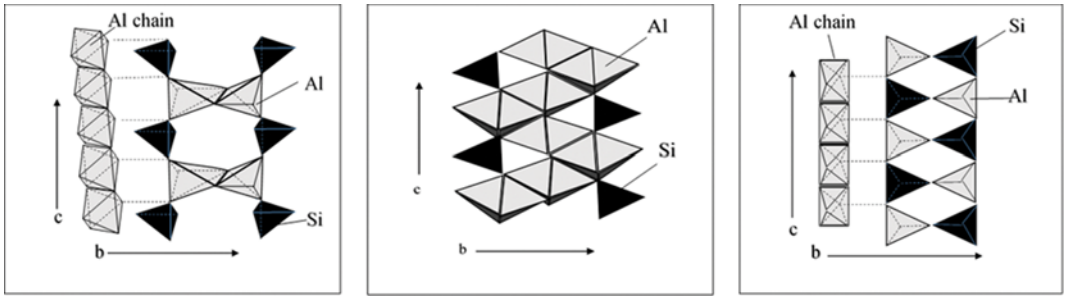

Fig. 1. The crystallography of Andalusite (left), Kyanite (center) and Sillimanite (right) minerals [40].

†To whom correspondence should be addressed.
E-mail: Seifpanahi@shahroodut.ac.ir, q.s11063@yahoo.com

fly ash [31], red mud [32], and zeolite [33]. Using natural adsorbent in nano scale will increase their efficiency because of particle size reduction and as a result, surface area increase [27]. Polymorphs of aluminosilicates are widely used as refractory materials. Andalusite is a raw material in the ceramic industry and high temperature applications [34]. Kyanite refractories are used in furnaces for smelting non-ferrous metals like copper, zinc and nickel alloys [35]. Sillimanite is a very good raw material for production of refractory breaks due to its high thermal shock resistance. Sillimanite-based refractory breaks are used in the lining of blast furnaces, soaking pits, reheating furnaces of iron and steel and rotary kilns of cement manufacturing [36,37].

Although three anhydrous aluminum silicate minerals, Andalusite, Kyanite and Sillimanite, are of same chemical composition, Al_2SiO_5, they have different crystal structures and physical properties [38,39]. The crystallography of these minerals is shown in Fig. 1.

Table 1. XRF analyze of ANPs, KNPs and SNPs

Analyte	ANPs (wt%)	KNPs (wt%)	SNPs (wt%)
Al_2O_3	46.31	40.82	34.41
SiO_2	34.37	32.13	38.35
Fe_2O_3	13.78	11.58	13.16
TiO_2	1.92	2.26	3.50
MgO	0.03	5.98	2.81
ZrO_2	0.31	3.09	2.14
CaO	0.75	0.68	0.86
MnO	0.02	0.27	0.15
P_2O_5	0.03	0.99	0.92
Na_2O	1.00	1.71	1.34
K_2O	1.48	0.49	1.75
Summation	100	100	100

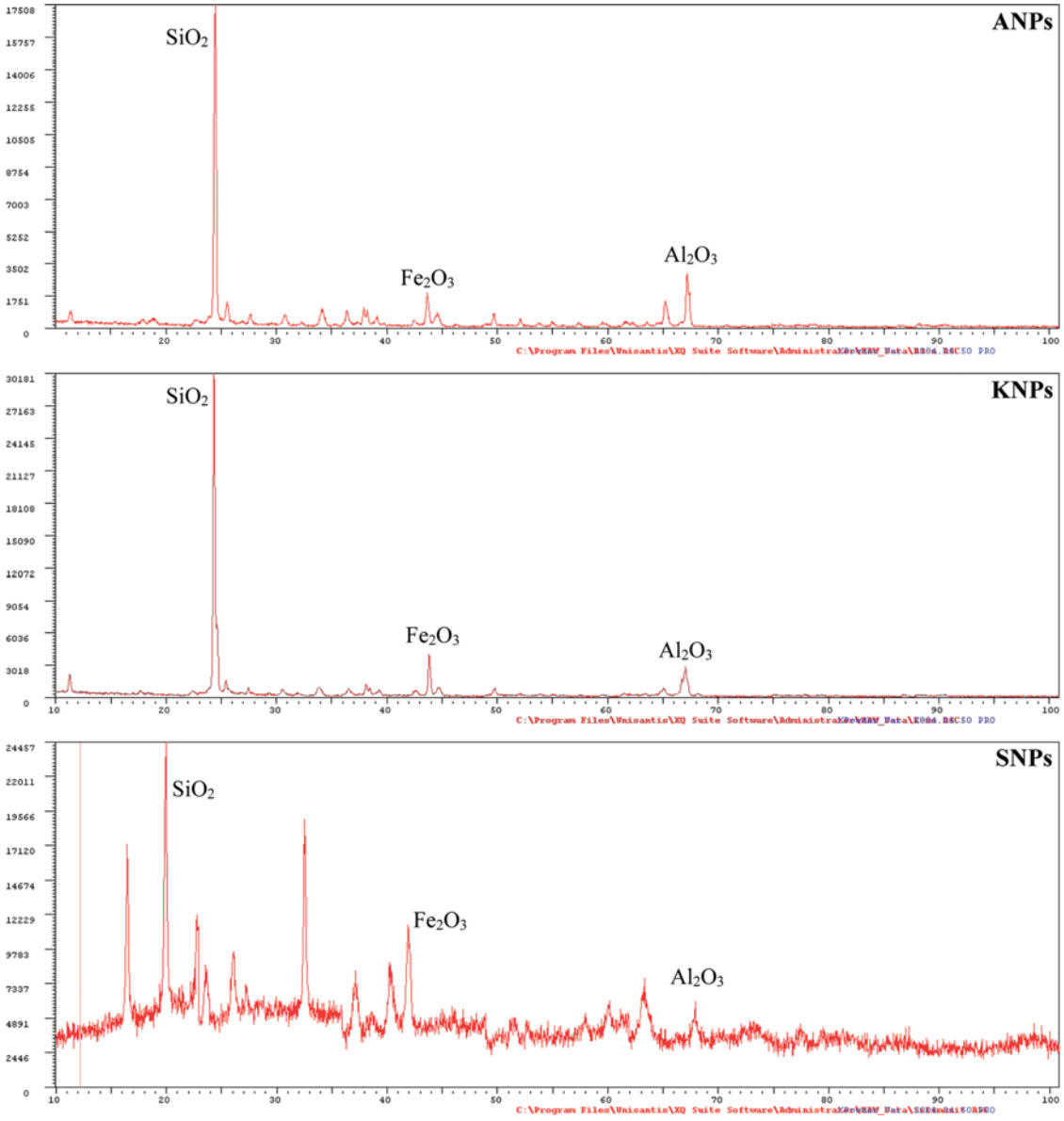

Fig. 2. XRD patterns of ANPs, KNPs and SNPs.

Based on Fig. 1, in Andalusite $Al^{[6]}Al^{[5]}SiO_5$, an orthorhombic polymorph, half the Al is found in octahedral chains and the other half occurs in 5-coordinated polyhedral which are linked by SiO_4 tetrahedra. For Kyanite $Al^{[6]}Al^{[6]}SiO_5$, the triclinic polymorph, all of the Al is octahedrally coordinated. It occurs as octahedral chains parallel to *c* and as isolated Al octahedral. Finally, in Sillimanite $Al^{[6]}Al^{[4]}SiO_5$, another orthorhombic polymorph, the octahedrally coordinated Al is found in octahedral chains and adjacent tetrahedral chains consist of alternating tetrahedral AlO_4 and SiO_4 groups [40].

Except for Andalusite, Kyanite and Sillimanite raw minerals reported of being used as an adsorbent [35,37,41,42], but not at nano scale. So, based on a literature review, the objectives of this study were preparation, characterization and utilization of Andalusite, Kyanite and Sillimanite as natural nano adsorbents for removal of disperse red 177 (DR-177) and disperse blue 60 (DB-60) dyes in the batch system.

MATERIALS AND METHODOLOGY

1. Materials

Andalusite, Kyanite and Sillimanite raw samples were obtained from internal sources in Hamadan aluminosilicate mine, Iran. DR-177 and DB-60 dyes and all other chemicals including sodium hydroxide and chloridric acid were manufactured by Merck Company.

2. Adsorbents Modification

Three adsorbents were washed by distilled water and then dried at 100 °C for eight hours. To reach the appropriate size, adsorbents were crushed using a planetary ball mill (Narva-MPM-2*250H model) in 550 RPM for five hours.

3. Nanoadsorbent Characterization

3-1. XRF Analysis

To investigate the chemical composition of modified Andalusite, Kyanite and Sillimanite nanoparticles (ANPs, KNPs and SNPs, respectively), they were analyzed through X-ray fluorescence (Shimadzu XRF-1800), as shown in Table 1.

Table 1 shows that the major components are Al_2O_3, SiO_2 and Fe_2O_3.

3-2. XRD Analysis

In the next stage, ANPs, KNPs and SNPs were analyzed through X-ray diffraction (XMD300-Unisantis). XRD patterns of ANPs, KNPs and SNPs are shown in Fig. 2.

According to Fig. 2 major peaks are SiO_2, Al_2O_3 and Fe_2O_3 components. XRD spectra for ANPs and KNPs have singular sharp peaks, but SNPs have a noisy spectra that is referred to as orthorhombic string morphology of SNPs (see Fig. 1).

3-3. SEM Image

Fig. 3 shows the surface morphology of modified ANPs, KNPs and SNPs using a scanning electron microscopy analysis (LEO-1455VP model).

Similar observation for three nanoadsorbents is obvious with granular, spherical and homogenous issue of particles and particle size less than 100 nm, totally.

3-4. FT-IR Spectra

FT-IR curves were drawn to demonstrate the presence of different functional groups on adsorbents surface. Fig. 4 shows FT-IR spectra of nanoadsorbents.

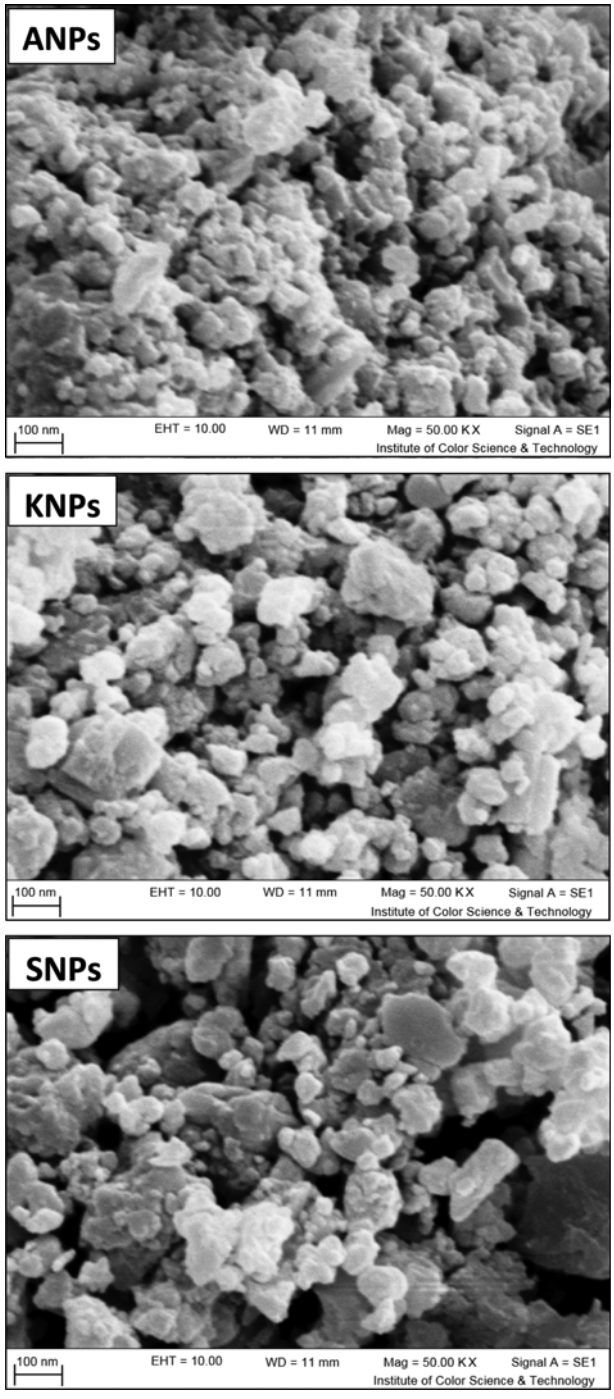

Fig. 3. SEM images of ANPs, KNPs and SNPs.

For ANPs, KNPs and SNPs seven main common absorption bands are observed at 458 cm^{-1} (B1), 607 cm^{-1} (B2), 976 cm^{-1} (B3), 1,398 cm^{-1} (B4), 1,629 cm^{-1} (B5), 3,128 cm^{-1} (B6) and 3,431 cm^{-1} (B7). Bands B1and B2 are deformation vibration of silica tetrahedron and the vibration of Al-O octahedron. Band B3 is attributed to symmetrical and asymmetrical vibration of silica tetrahedron [43]. Band B4 is the deformation band of molecular water. Band

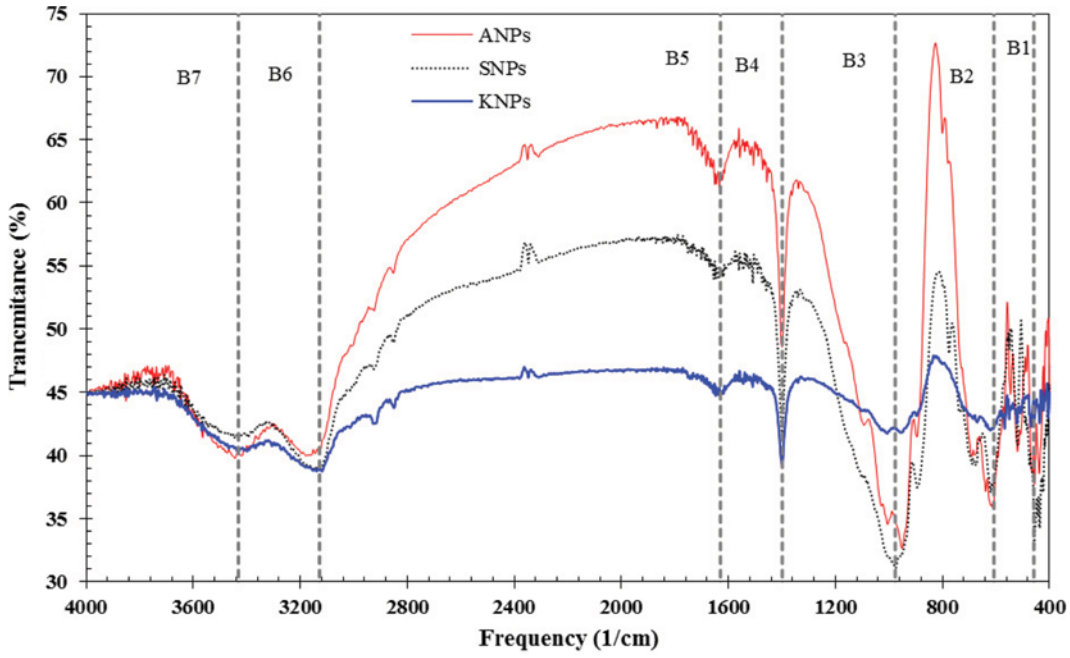

Fig. 4. FT-IR spectra of ANPs, KNPs and SNPs.

B5 is attributed to molecular adsorbed water. Band B6 is OH related [44]. Band B7 is related to OH defects on oxygen sites [45]. The intensity of B4, B5 and B6 bands is closely related to the water content, similar to other silicate materials, such as volcanic tuffs, diatomite, perlite and zeolites [27].

4. Experimental Studies

4-1. Batch Mode

Experiments were carried out with 250 ml of synthetic dye solutions volume. In each test 0.5 g of adsorbents was used in 100 mg/*l* of dye concentrations under room temperature and desired pH, except for those of which were done to find the effects of respective factor. The pH of dye solutions was adjusted using 1.0 M NaOH and 1.0 M HCl solutions, measured with a digital pH meter (AZ pH/mV/Temp. meter. 86502). Initial dye and adsorbents concentrations effects were studied for 50, 100, 150 and 200 mg/*l* of each dye and 0.1, 0.2, 0.3, 0.4 and 0.5 g of each adsorbent, respectively. Finally the effects of temperature change were investigated using a hot plate to adjust the temperature. Samples were taken at time intervals of 10, 20, 40, 60, 80, 100 and 120 min and then centrifuged. The amount of dye concentrations was measured by spectrophotometer (UV Visible/2100, Unico, USA) corresponding to their maximum absorbance. The percentage removal of dyes was computed by Eq. (1):

$$\text{Removal}\ (\%) = \left(\frac{C_0 - C_t}{C_0}\right) \times 100 \quad (1)$$

where C_0 and C_t are initial concentration and concentration at time, respectively. The amount of dye adsorbed at equilibrium (mg/g) was calculated by a mass-balance relationship:

$$q_e = \frac{(C_0 - C_e) \times V}{m} \quad (2)$$

where, C_0 and C_e are the initial and equilibrium dye concentration, respectively (mg/*l*), V is the volume of solution (mL) and m is the adsorbents dosage (g).

4-2. Effect of pH

The pH of the solution plays an important role in adsorption process, affecting adsorbent surface charge. In Fig. 5, the effect of pH on removal of DR-177 dye by ANPs (a), KNPs (b), SNPs (c) and DB-60 dye by ANPs (d), KNPs (e) and SNPs (f) is shown.

According to Fig. 5, the effect of pH on dye removal indicates the maximum uptake occurs at pH 2. Many researchers reported that adsorption of disperse dyes best happens at acidic pH [9,24-26,46]. Two factors may cause this phenomenon. First, disperse dyes are non-ionic and are negatively charged in solution. At low pH, the adsorbent surface is positively charged. So high adsorption capacity is due to high electrostatic interaction between negative dye particles and positive adsorbent surface as well as lower amount of OH^- ions at acidic pH values. Increase of the pH parameter would change the adsorbent surface charge negatively and also increase OH^- ions competing with anionic dye molecules for the adsorbent sites [24-26]. The second parameter is hydrophobic reaction, which is due to hydrophobicity of disperse dyes. So they show higher affinity for solid surfaces than for water [47].

4-3. Effect of Initial Dye Concentration

As mentioned, initial concentration of DR-177 and DB-60 dyes was changed in the 50-200 mg/L ranges. The effect of variability of initial dye concentration on the adsorption process is shown in Fig. 6.

It is clear that with an increase of dye concentration, adsorption capacity decreased. This can be explained by the fact that the adsorbent has a limited number of activated sites. At low concentrations the ratio of surface active sites to the total dye molecules is high, but with increased dye concentrations, the number of active

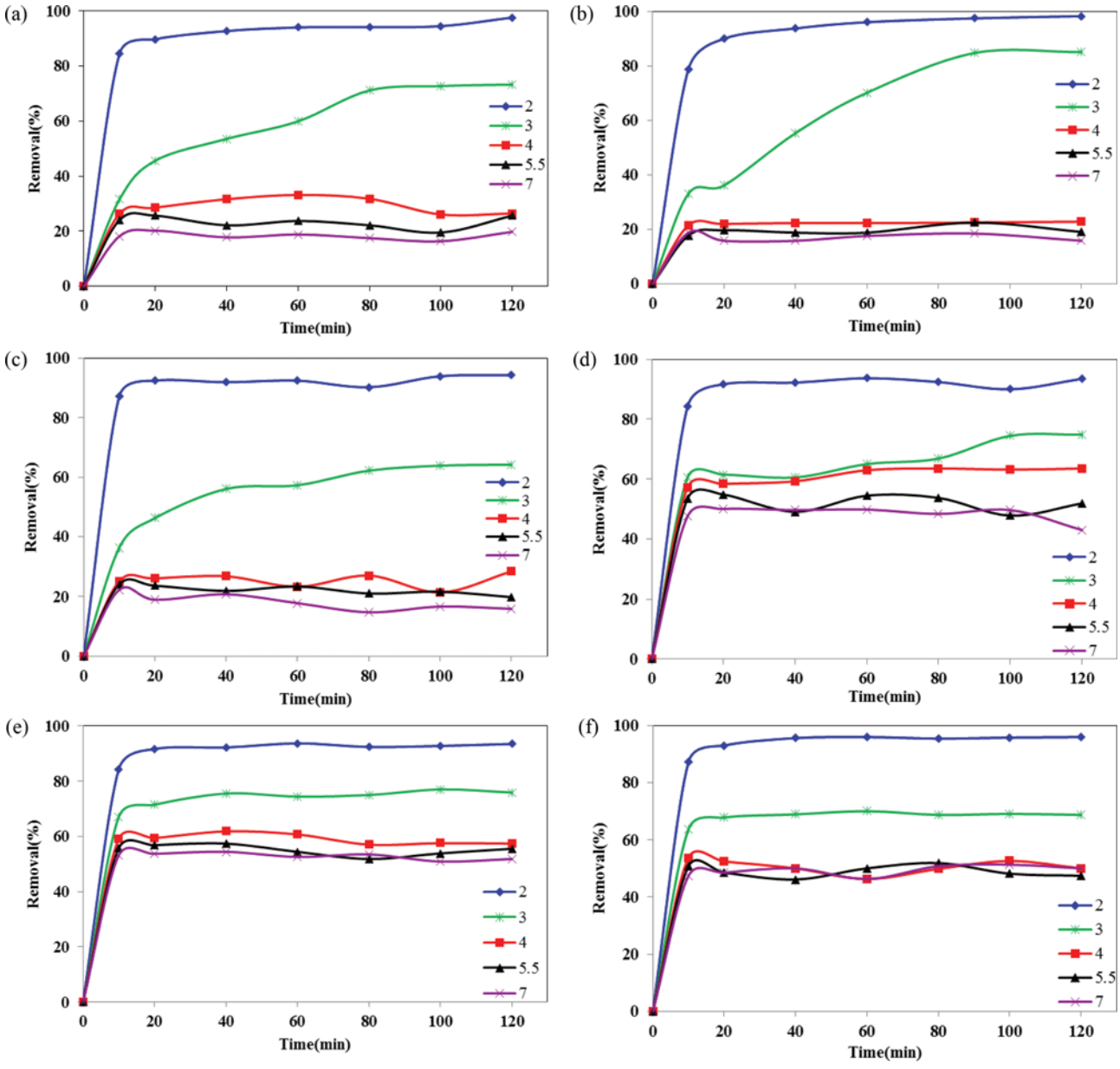

Fig. 5. Effect of pH on removal of DR-177 dye by ANPs (a), KNPs (b), SNPs (c) and DB-60 dye by ANPs (d), KNPs (e) and SNPs (f).

adsorption sites is not enough to accommodate dye molecules [24].

4-4. Effect of Initial Adsorbents Dosage

Based on Fig. 7, which shows the effect of initial adsorbent concentration on removal of dyes, it can be inferred that increasing the amount of adsorbent will increase the percentage of dye removal. This indicates that increase of adsorbent dose increases the sorption surface. Maximum uptake happens at 0.5 g adsorbent dosage. Although all dosages are successful in removing dyes and they reach the equilibrium after 90 min except for 0.1 g, but higher amounts have higher rapidity.

4-5. Effect of Temperature

The effect of temperature on DR-177 and DB-60 dyes removal from aqueous solution was considered for 283, 294, 303 and 313 °K. The results of temperature changes are shown in Fig. 8.

According to Fig. 8, the percentage removal with respect to time for 283, 294, 303 and 313 °K, rise of temperature can accelerate the adsorption process and reduce the equilibrium time.

5. Adsorption Isotherms

Equilibrium data, commonly known as adsorption isotherms, are the basic requirements for the design of adsorption systems. Obtaining equilibrium for a specific adsorbate-adsorbent system can be performed experimentally with a time-consuming procedure [48]. In addition to Langmuir and Freundlich, the two most commonly isotherms, the Temkin isotherm also has been used to analyze the equilibrium data.

The Langmuir isotherm model assumes that sorption takes place at specific homogeneous sites within the adsorbent. Thus, the

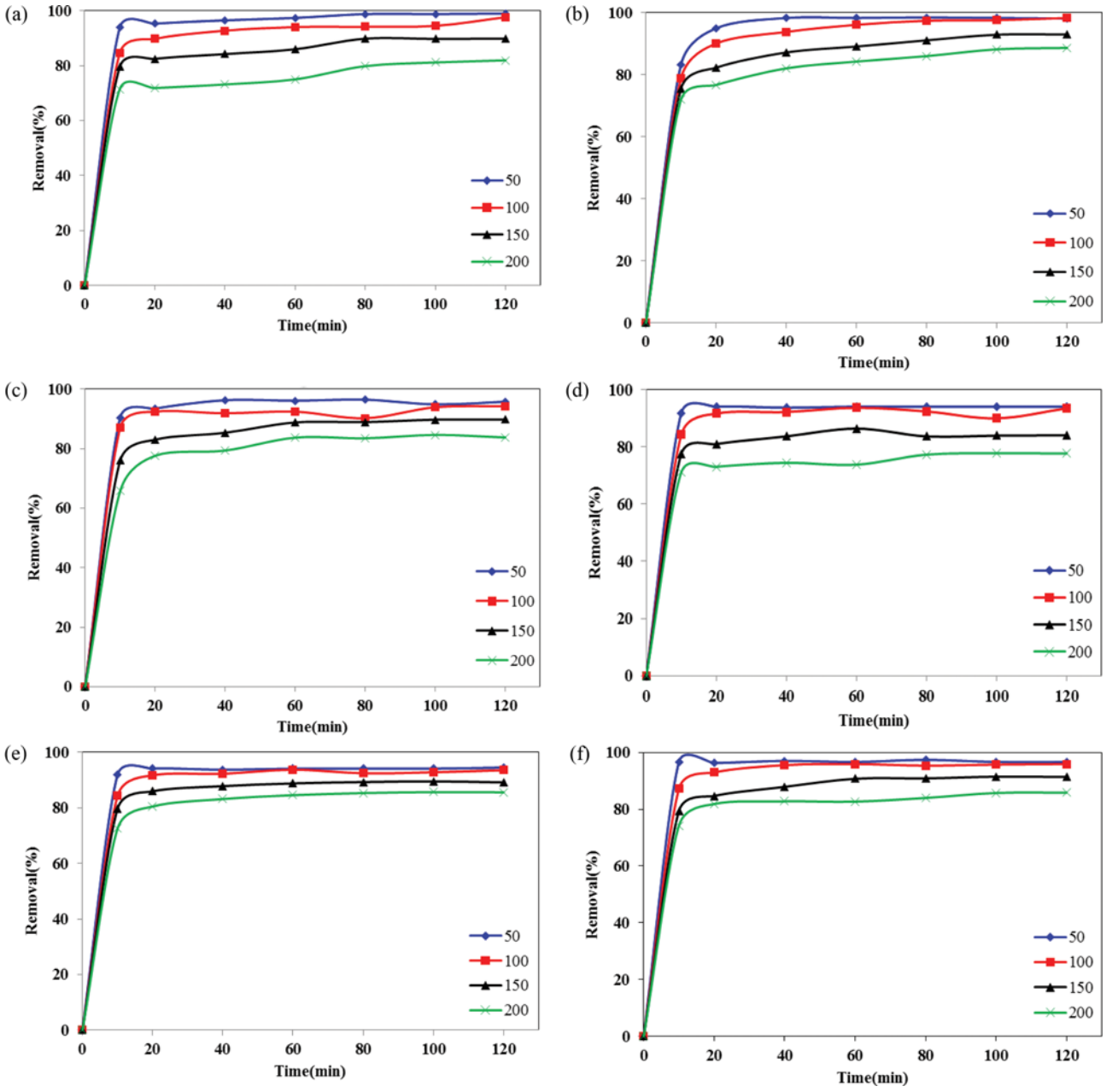

Fig. 6. Effect of initial dye concentration on removal percentage of DR-177 dye by ANPs (a), KNPs (b), SNPs (c) and DB-60 dye by ANPs (d), KNPs (e) and SNPs (f).

adsorption process is monolayer based. While, the Freundlich model is based on multilayered adsorption on a heterogeneous surface [49]. Temkin isotherm model assumes that heat of sorption of all molecules in the layer decreases linearly with coverage due to sorbate-sorbate interactions, and sorption is characterized by a uniform distribution of binding energies, up to some maximum binding energy. It indicates that the fall in the heat of sorption is linear rather than logarithmic as implied in Freundlich equation [50]. Table 2 shows the models and their linear forms.

In Table 2, q_e is the amount adsorbed at equilibrium (mg/g) and C_e is the equilibrium concentration of solution (mg/*l*). For the Langmuir isotherm, q_m is a constant related to the area occupied by a monolayer of the adsorbate, reflecting the maximum adsorption capacity (mg/g) and K_L is a direct measure of the intensity of adsorption (*l*/mg). In the Freundlich isotherm, K_F ((mg/g) (*l*/mg)$^{1/n}$ and n (dimensionless) are constants incorporating all factors affecting the adsorption process, such as adsorption capacity and intensity, respectively. In the Temkin isotherm, R is the gas constant (8.314 J/Mol K), T is the absolute temperature (K), K_T is the equilibrium binding constant (*l*/mg) and b is the Temkin constant related to the heat of sorption (J/Mol). In Fig. 9, the diagrams of isotherm modeling are shown.

Equilibrium data for the adsorption of DR-177 dye and DB-60 dye by ANPs, KNPs and SNPs are shown in Table 3.

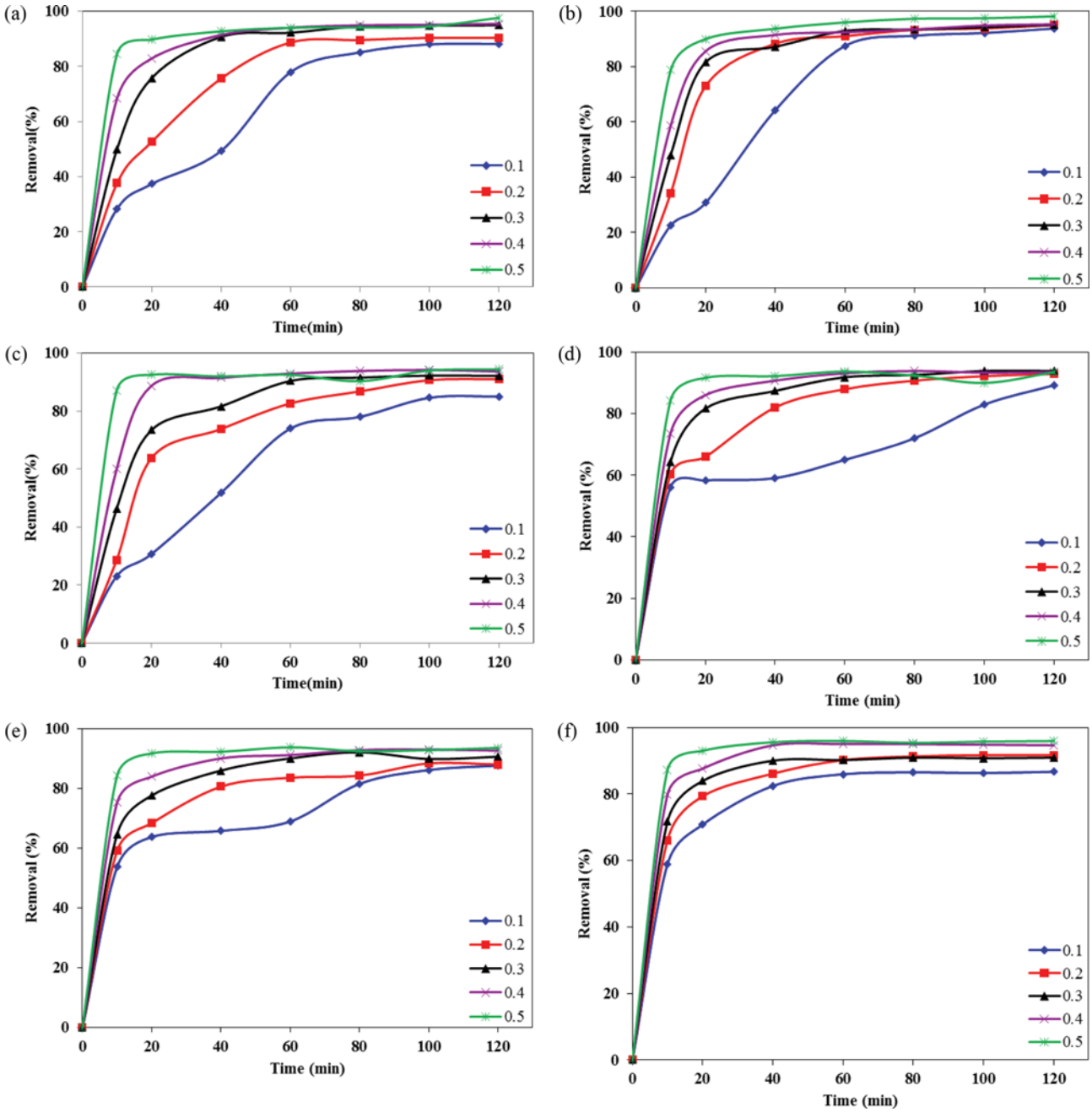

Fig. 7. Removal of DR-177 dye with respect to concentration of ANPs (a), KNPs (b) and SNPs (c) and also DB-60 dye by ANPs (d), KNPs (e) and SNPs (f).

According to Table 3, the adsorption of DB-60 dye by KNPs and SNPs follows the Freundlich isotherm model, but for ANPs, the Temkin isotherm has a better correlation. Also, adsorption of DR-177 dye by KNPs and SNPs obeys the Temkin isotherm model, and by ANPs, follows the Freundlich isotherm. This is due to their high correlation coefficient (R^2), which proves a great fitness.

6. Adsorption Kinetics

6-1. Pseudo-first and Pseudo-second-order Kinetic Models

Adsorption kinetic studies are important in the treatment of aqueous effluents because they provide valuable information about the mechanism of the adsorption process [52]. Thus, pseudo-first-order and pseudo-second-order kinetic models were used to model the adsorption kinetic of DR-177 dye and DB-60 dye on ANPs, KNPs and SNPs. The agreement of experimental data and the model predicted values is expressed by the correlation coefficients (R^2). The models are listed in Table 4.

In Table 4, q_e and q_t are the amounts of metal ions adsorbed on the adsorbent (mg/g) at equilibrium and at time t, respectively, k_1 is the rate constant of first-order adsorption (min^{-1}) and k_2 is the rate constant of second-order adsorption (g/(mg min)). The diagrams for isotherm modeling of pseudo-first and second order are shown in Fig. 10.

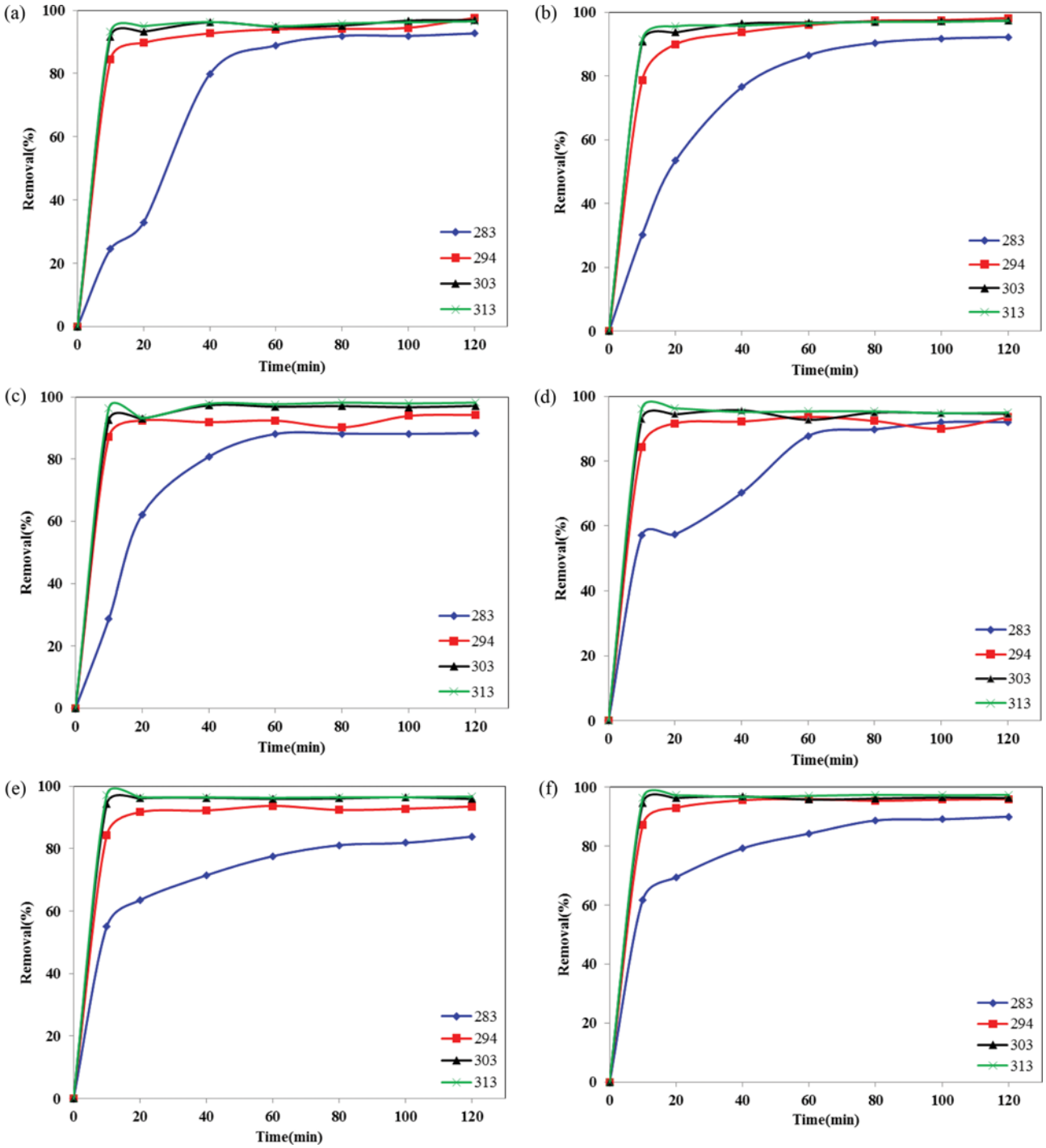

Fig. 8. Effect of temperature on removal of DR-177 dye by ANPs (a), KNPs (b), SNPs(c) and DB-60 dye by ANPs (d), KNPs (e) and SNPs (f).

Table 2. Isotherm models and their linear forms [51]

Isotherm model	Equation	A linear form	Plot
Langmuir	$q_e = \frac{q_m K_L C_e}{1 + K_L C_e}$	$\frac{C_e}{q_e} = \frac{1}{K_L q_m} + \frac{1}{q_m} C_e$	$\frac{C_e}{q_e}$ vs. C_e
Freundlich	$q_e = K_F C_e^{1/n}$	$\ln(q_e) = \ln K_F + \frac{1}{n} \ln C_e$	$\ln q_e$ vs. $\ln C_e$
Temkin	$q_e = \frac{RT}{b} \ln(K_T C_e)$	$q_e = \frac{RT}{b} \ln K_T + \frac{RT}{b} \ln C_e$	q_e vs. $\ln C_e$

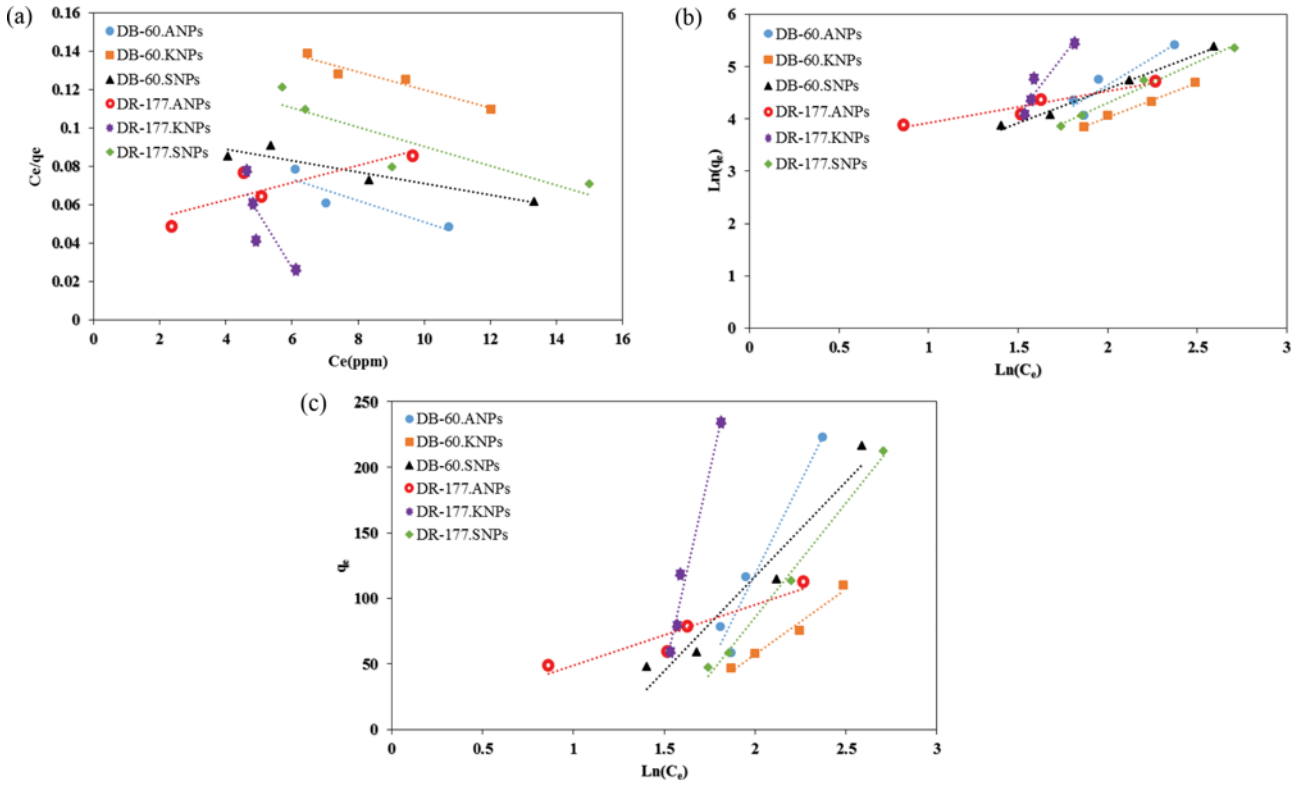

Fig. 9. Isotherm modeling diagrams of Langmuir (a), Freundlich (b) and Temkin (c).

Table 3. Langmuir, Freundlich and Temkin isotherm parameters on adsorption of DR-177 dye and DB-60 dye by ANPs, KNPs and SNPs

Adsorbent	Dye	Langmuir			Freundlich			Temkin		
		q_m (mg/g)	K_L	R^2	K_F	n	R^2	B_1	K_T	R^2
ANPs	DB-60	178.571	0.052	0.825	1.576	0.477	0.851	280.110	4.836	0.948
	DR-177	222.222	0.102	0.751	27.500	1.643	0.924	46.354	1.054	0.897
KNPs	DB-60	212.766	0.028	0.933	3.815	0.744	0.994	99.667	4.152	0.973
	DR-177	35.714	0.143	0.171	13.682	0.223	0.898	613.990	4.173	0.973
SNPs	DB-60	333.333	0.030	0.881	7.122	0.763	0.991	144.160	3.283	0.942
	DR-177	200.000	0.035	0.792	3.264	0.640	0.987	173.400	4.500	0.994

Table 4. Kinetic models and their linear form [27]

Kinetic model	Equation	A linear form	Plot
Pseudo-first-order	$\frac{dq_t}{dt}=k_1(q_e-q_t)$	$\ln(q_e-q_t)=\ln q_e-k_1 t$	$\ln(q_e-q_t)$ vs. t
Pseudo-second-order	$\frac{dq_t}{dt}=k_2(q_e-q_t)^2$	$\frac{t}{q_t}=\frac{1}{k_2 q_e^2}+\frac{1}{q_e}t$	$\frac{t}{q_t}$ vs. t

The values of parameters obtained by kinetic models together with the amount of adsorption at equilibrium (q_e Exp) are shown in Table 5.

According to Table 5, from a high value of correlation coefficients as well as the agreement of calculated and experimental q_e, it can be demonstrated that the adsorption of DR-177 and DB-60 dyes follows a pseudo-second-order kinetic model. Therefore, chemisorption may be the rate limiting step [27].

6-2. Intraparticle Diffusion Model

It is generally known that a typical liquid/solid adsorption involves film diffusion, intraparticle diffusion and mass action. For kinetic study, mass action is very rapid and can be neglected. Thus the kinetic process of adsorption is always controlled by film or intraparticle diffusion, i.e., one of them should be the rate limiting step

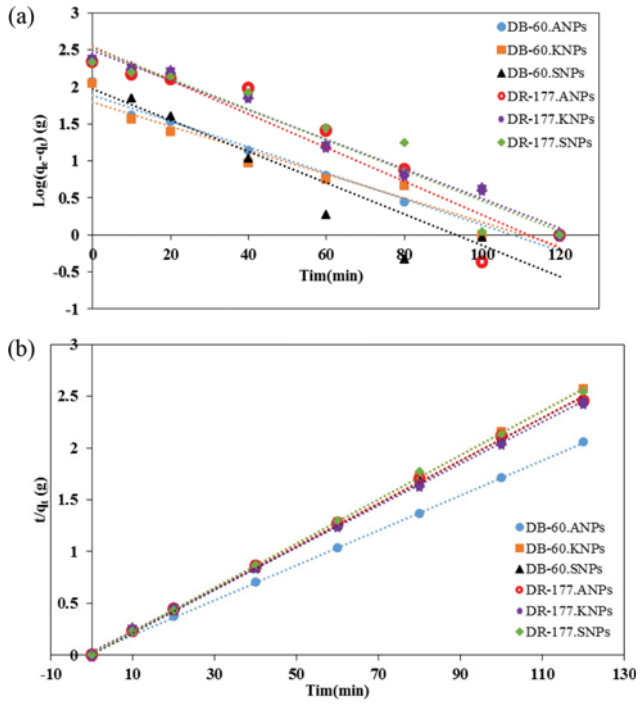

Fig. 10. Diagrams of pseudo-first-order (a) and pseudo-second-order (b) kinetic modeling.

[53]. Intraparticle diffusion model [54] can be defined as:

$$q_t = \frac{k_i}{m} t^{0.5} + C$$

where C is the intercept and related to the thickness of boundary layer, m is the mass of sorbent (g), q_t the amount of solute adsorbed at time t (mg/g), and K_i is the initial rate of intraparticle diffusion (mg/(*l* $s^{1/2}$)). In case of intraparticle diffusion model, the plot of q_t vs. square root of contact time may result a straight line, passing through the origin, indicating that the intraparticle diffusion is the sole rate limiting step [55]. Such plots are shown in Fig. 11.

Fig. 11 presents multiline plots [25,26], showing that two steps are occurring. All plots contain an initial linear portion followed by a plateau. The initial linear portion is the gradual adsorption stage where intraparticle diffusion is rate controlled, and the following portion is the final equilibrium stage where intraparticle diffusion slows down due to the low concentration in the solution. The intercept values show the possibility of some boundary layer

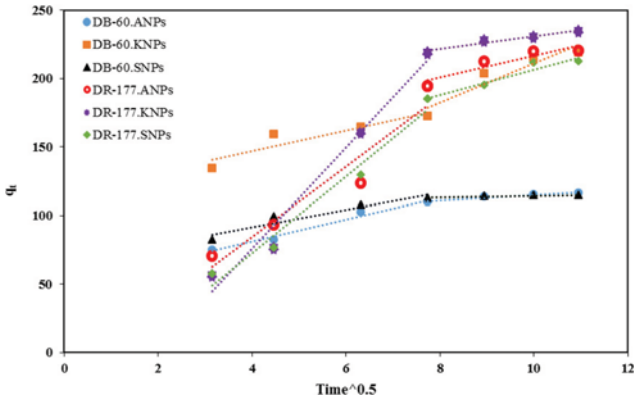

Fig. 11. Intraparticle diffusion kinetics of DR-177 and DB-60 dyes onto ANPs, KNPs and SNPs.

Table 6. Parameters of intraparticle diffusion model for the adsorption of DR-177 and DB-60 dyes onto ANPs, KNPs and SNPs

Adsorbent	Dye	K_{i1}	r_1^2	K_{i2}	r_2^2
ANPs	DB-60	8.036	0.980	1.951	0.952
	DR-177	25.618	0.920	8.052	0.858
KNPs	DB-60	7.464	0.844	14.480	0.886
	DR-177	36.917	0.975	4.705	0.945
SNPs	DB-60	6.265	0.920	0.577	0.826
	DR-177	27.918	0.972	9.364	0.934

operation. The external surface portion, film diffusion, is absent due to completion before ten minutes.

From the slopes of linear parts in Fig. 11, the values of K_i can be estimated. These values are presented in Table 6.

To prove the absence of film diffusion step, the experimental data was plotted, using the Boyd equation. If the plots are linear and pass through origin, then the slowest (rate controlling) step in the adsorption process is the internal diffusion [56]. Fig. 12 presents the Boyd plot.

The results indicate the fitness of intraparticle diffusion model for the initial linear portion only, but the pseudo-second-order kinetic model for the whole adsorption process.

7. Thermodynamic Study

The effect of temperature on the adsorption of DR-177 and DB-60 dyes onto ANPs, KNPs and SNPs was estimated by deter-

Table 5. Pseudo-first and second order kinetic model parameters for adsorption of DR-177 and DB-60 dyes onto ANPs, KNPs and SNPs

Adsorbent	Dye	Pseudo-first-order			Pseudo-second-order			q_e Exp. (mg/g)
		K_1 (1/min)	q_e (mg/g)	R^2	K_2 (g/mg/min)	q_e (mg/g)	R^2	
ANPs	DB-60	0.037	13.896	0.634	0.011	59.171	0.999	58.449
	DR-177	0.023	11.598	0.679	0.015	48.543	0.999	48.816
KNPs	DB-60	0.024	5.593	0.460	0.043	46.729	0.999	46.759
	DR-177	0.033	13.225	0.739	0.012	49.505	0.999	49.123
SNPs	DB-60	0.030	5.360	0.449	0.042	48.077	0.999	47.963
	DR-177	0.024	6.162	0.440	0.030	46.948	0.999	47.149

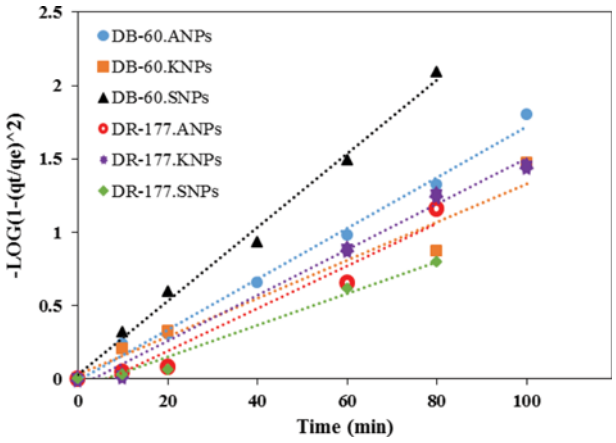

Fig. 12. Boyd plot for the adsorption of DR-177 and DB-60 dyes onto ANPs, KNPs and SNPs.

mining the free energy change (ΔG^0), enthalpy change (ΔH^0) and entropy change (ΔS^0). Thermodynamic parameters were calculated using the following equations [57-59]:

$$K_d = \frac{q_e}{C_e} \quad (4)$$

$$\Delta G^o = -RT\ln K_d \quad (5)$$

$$\ln K_d = \frac{\Delta S^o}{R} - \frac{\Delta H^o}{R}\frac{1}{T} \quad (6)$$

$$\Delta G^o = \Delta H^o - T\Delta S^o \quad (7)$$

where K_d is the equilibrium constant (L/mol), R is the gas constant (8.314 J/mol K) and T is the temperature (K). Considering the relationship between ΔG^0 and K_d, ΔH^0 and ΔS^0 were determined from the slope and intercept of the van't Hoff plots of $\ln(K_d)$ vs. 1/T.

Calculated thermodynamic parameters are presented in Table 7.

Negative values of ΔG^0 confirm the spontaneous nature of the adsorption process. Also, the increase in the negative ΔG^0 values with an increase of temperature indicates that the adsorption becomes more favorable at higher temperatures. For all the reactions, enthalpy values are negative, showing that the adsorption process is exothermic. Low positive values of entropy prove low randomness at the solid/solution interface.

CONCLUSION

Three anhydrous aluminum silicate minerals, Andalusite, Kyanite and Sillimanite, were used as nanoadsorbents for removal of DR-177 and DB-60 dyes. All the adsorbents were characterized using FT-IR, XRD, XRF and SEM analyses. The results of XRF and XRD analyses show that the major components are Al_2O_3, SiO_2 and Fe_2O_3. SEM analysis proves particle size less than 100 nm with granular, spherical and homogeneous issue of particles. Finally, FT-IR analysis was used to demonstrate the presence of different functional groups on adsorbents surfaces. This study proved that ANPs, KNPs and SNPs have a high adsorption capacity and adsorption rate for the DR-177 and DB-60 dyes adsorption. Therefore, they are potential candidates for the removal of dyes from wastewaters. During this research, the adsorption of DR-177 and DB-60 dyes onto ANPs, KNPs and SNPs minerals was investigated, based on the effects of pH, initial dye concentration, adsorbent dosage and temperature. Further studies were done calculating isotherm and kinetic models as well as thermodynamic parameters. The optimal pH was 2 and an increase of initial dye concentration, adsorbent dosage and temperature had a negative, positive and positive effect on the adsorption, respectively. Temkin and Freundlich isotherms could describe the equilibrium data. The calculated data showed better correlation with pseudo-second-order kinetic model for the whole process, while the intraparticle diffusion model fitted just for the primary portion. Thermodynamic parameters value reflected the spontaneous, exothermic nature of the adsorption process and low randomness at the solid/solution interface.

ACKNOWLEDGEMENTS

Shahrood University of Technology is acknowledged for the great support of this research. Also, we appreciate Mr. Mohammad Kabirian for any unsparing help.

REFERENCES

1. F. Kong, K. Parhiala, S. Wang and P. Fatehi, *Eur. Polym. J.*, **67**, 335 (2015).
2. M. N. Mahamad, M. A. A. Zaini and Z. A. Zakaria, *Int. Biodeterior. Biodegrad.*, **102**, 274 (2015).
3. M. Shanehsaz, S. Seidi, Y. Ghorbani, S. M. R. Shoja and S. Rouhani, *Spectrochim. Acta Part A Mol. Biomol. Spectrosc.*, **149**, 481 (2015).
4. N. Ghaemi, S. S. Madaeni, P. Daraei, H. Rajabi, T. Shojaeimehr, F. Rahimpour and B. Shirvani, *J. Hazard. Mater.*, **298**, 111 (2015).
5. M. T. Yagub, T. K. Sen, S. Afroze and H. M. Ang, *Adv. Colloid*

Table 7. Values of thermodynamic parameters for adsorption of DR-177 and DB-60 dyes onto ANPs, KNPs and SNPs

Adsorbent	Dye	ΔH (kJ/mol)	ΔS (J/mol K)	ΔG (kJ/mol)			
				283 °K	294 °K	303 °K	313 °K
ANPs	DB-60	−8.668	0.060	−25.609	−26.267	−26.806	−27.405
	DR-177	−11.521	0.050	−25.403	−25.943	−26.384	−26.875
KNPs	DB-60	−38.667	0.040	−49.725	−50.155	−50.507	−50.897
	DR-177	−15.098	0.036	−25.451	−25.853	−26.182	−26.548
SNPs	DB-60	−19.979	0.020	−25.861	−26.090	−26.277	−26.485
	DR-177	−28.371	0.007	−30.254	−30.327	−30.387	−30.453

Interface Sci., **209**, 172 (2014).
6. K. B. Tan, M. Vakili, B. A. Horri, P. E. Poh, A. Z. Abdullah and B. Salamatinia, *Sep. Purif. Technol.*, **150**, 229 (2015).
7. E. H. Ezechi, S. R. B. M. Kutty, A. Malakahmad and M. H. Isa, *Process Saf. Environ. Prot.*, **98**, 16 (2015).
8. B. Kayranli, *Chem. Eng. J.*, **173**, 782 (2011).
9. M. Hasnain Isa, L. Siew Lang, F. a. H. Asaari, H. a. Aziz, N. Azam Ramli and J. P. a. Dhas, *Dye. Pigment.*, **74**, 446 (2007).
10. Ö. Gerçel, H. F. Gerçel, a. S. Koparal and Ü. B. Öğütveren, *J. Hazard. Mater.*, **160**, 668 (2008).
11. B. Merzouk, B. Gourich, K. Madani, C. Vial and A. Sekki, *Desalination*, **272**, 246 (2011).
12. V. Golob and A. Ojstršek, *Dye. Pigment.*, **64**, 57 (2005).
13. K. Shi and I. Zhitomirsky, *Electrochim. Acta*, **174**, 588 (2015).
14. M. R. S. Kebria, M. Jahanshahi and A. Rahimpour, *Desalination*, **367**, 255 (2015).
15. S. Sirianuntapiboon and P. Srisornsak, *Bioresour. Technol.*, **98**, 1057 (2007).
16. Z. Chen, J. Zhang, J. Fu, M. Wang, X. Wang, R. Han and Q. Xu, *J. Hazard. Mater.*, **273**, 263 (2014).
17. A. a. El-Bindary, M. a. Hussien, M. a. Diab and A. M. Eessa, *J. Mol. Liq.*, **197**, 236 (2014).
18. C. A. Demarchi, M. Campos and C. A. Rodrigues, *J. Environ. Chem. Eng.*, **1**, 1350 (2013).
19. B. Feng, X. Xu, W. Xu, G. Zhou, J. Hu, Y. Wang and Z. Bao, *Mater. Des.*, **83**, 522 (2015).
20. R. F. Gomes, A. C. N. de Azevedo, A. G. B. Pereira, E. C. Muniz, A. R. Fajardo and F. H. a. Rodrigues, *J. Colloid Interface Sci.*, **454**, 200 (2015).
21. R. Wang, M. Xie, H. Wang, X. Shi and C. Lei, *Korean J. Chem. Eng.*, **33**, 976 (2016).
22. A. A. Ahmad, B. H. Hameed and a. L. Ahmad, *J. Hazard. Mater.*, **170**, 612 (2009).
23. M. A. M. Salleh, D. K. Mahmoud, W. A. W. A. Karim and A. Idris, *Desalination*, **280**, 1 (2011).
24. L. Wang, *J. Environ. Manage.*, **102**, 79 (2012).
25. M. Özacar and I. A. Sengil, *Colloids Surfaces A Physicochem. Eng. Asp.*, **242**, 105 (2004).
26. Q. Y. Yue, Q. Li, B. Y. Gao and Y. Wang, *Sep. Purif. Technol.*, **54**, 279 (2007).
27. K. Seifpanahi Shabani, F. Doulati Ardejani, K. Badii and M. E. Olya, *Arab. J. Chem.*, Article in Press (2013).
28. K. Vijayaraghavan and F. D. Raja, *J. Water Process Eng.*, **4**, 179 (2014).
29. L. Xu, X. Gao, Z. Li and C. Gao, *Desalination*, **369**, 97 (2015).
30. a. Vinati, B. Mahanty and S. K. Behera, *Appl. Clay Sci.*, **114**, 340 (2015).
31. Q. Zhou, Y. Duan, C. Zhu, J. Zhang, M. She, H. Wei and Y. Hong, *Korean J. Chem. Eng.*, **32**, 1405 (2015).
32. T. A. Khan, S. a. Chaudhry and I. Ali, *J. Mol. Liq.*, **202**, 165 (2015).
33. V. Simon, a. Thuret, L. Candy, S. Bassil, S. Duthen, C. Raynaud and a. Masseron, *Chem. Eng. J.*, **280**, 748 (2015).
34. T. Wala, B. Psiuk, J. Kubacki, K. Stec and J. Podwórny, *Ceram. Int.*, **40**, 5129 (2014).
35. M. Ajmal, R. K. Rao, R. Ahmad, J. Ahmad and L. K. Rao, *J. Hazard. Mater.*, **87**, 127 (2001).
36. S. Prabhakar, G. Bhaskar Raju and S. Subba Rao, *Int. J. Miner. Process.*, **81**, 159 (2006).
37. T. V. V. Kumar, S. Prabhakar and G. B. Raju, *J. Colloid Interface Sci.*, **247**, 275 (2002).
38. L. C. Zhou and Y. M. Zhang, *Trans. Nonferrous Met. Soc. China English Ed.*, **21**, 1388 (2011).
39. G. Bulut and C. Yurtsever, *Int. J. Miner. Process.*, **73**, 29 (2004).
40. C. Klien, B. Dutrow and J. Dana, The 23rd Ed. of the Manual of Mineral Science. Hoboken: Wiley (2008).
41. R. A. K. Rao, M. A. Khan and B. H. Hameed, *Chem. Eng. J.*, **152**, 421 (2009).
42. C. Varlikli, V. Bekiari, M. Kus, N. Boduroglu, I. Oner, P. Lianos, G. Lyberatos and S. Icli, *J. Hazard. Mater.*, **170**, 27 (2009).
43. H. Zhu, H. Deng and C. Chen, *Trans. Nonferrous Met. Soc. China*, **25**, 1279 (2015).
44. R. Karanth, *Gondwana Res.*, **2**, 89 (1999).
45. M. Wildner, A. Beran and F. Koller, *Mineral. Petrol.*, **107**, 289 (2013).
46. U. Tezcan, F. Ates, N. Erginel, O. Ozcan and E. Oduncu, *J. Environ. Manage.*, **155**, 89 (2015).
47. Q. Li, Q. Yue, Y. Su and B. Gao, *Bioresour. Technol.*, **102**, 5290 (2011).
48. B. Noroozi and G. Sorial, *J. Environ. Sci. (China)*, **25**, 419 (2013).
49. Y. Hai, X. Li, H. Wu, S. Zhao, W. Deligeer and S. Asuha, *Appl. Clay Sci.*, **114**, 558 (2015).
50. J. Shah, M. R. Jan, A. U. Haq and M. Zeeshan, *J. Saudi Chem. Soc.*, **19**, 301 (2015).
51. M. Najafi, Y. Yousefi and a. a. Rafati, *Sep. Purif. Technol.*, **85**, 193 (2012).
52. F. M. Machado, C. P. Bergmann, T. H. M. Fernandes, E. C. Lima, B. Royer, T. Calvete and S. B. Fagan, *J. Hazard. Mater.*, **192**, 1122 (2011).
53. H. Qiu, L. Lv, B. Pan, Q. Zhang, W. Zhang and Q. Zhang, *J. Zhejiang Univ. Sci. A*, **10**, 716 (2009).
54. A. a. Yakout and H. M. Albishri, *J. Taiwan Inst. Chem. Eng.*, **55**, 180 (2015).
55. F. Nekouei, H. Noorizadeh, S. Nekouei, M. Asif, I. Tyagi, S. Agarwal and V. K. Gupta, *J. Mol. Liq. Sep.*, **213**, 360 (2015).
56. C. O. Ijagbemi, M.-H. Baek and D.-S. Kim, *J. Hazard. Mater.*, **166**, 538 (2009).
57. M. Arshadi, *J. Mol. Liq.*, **211**, 899 (2015).
58. O. Moradi, V. K. Gupta, S. Agarwal, I. Tyagi, M. Asif, A. S. H. Makhlouf, H. Sadegh and R. Shahryari-ghoshekandi, *J. Ind. Eng. Chem.*, **28**, 294 (2015).
60. O. Duman, S. Tunç and T. G. Polat, *Appl. Clay Sci.*, **109-110**, 22 (2015).